A Methodology for Deblurring and Recovering Conformational States of Biomolecular Complexes from Single Particle Electron Microscopy

Bijan Afsari(✉) and Gregory S. Chirikjian

Johns Hopkins University, Baltimore, USA
bijan@cis.jhu.edu, gchirik1@jhu.edu

Abstract. In this paper we study two forms of blurring effects that may appear in the reconstruction of 3D Electron Microscopy (EM), specifically in single particle reconstruction from random orientations of large multi-unit biomolecular complexes. We model the blurring effects as being due to independent contributions from: (1) variations in the conformation of the biomolecular complex; and (2) errors accumulated in the reconstruction process. Under the assumption that these effects can be separated and treated independently, we show that the overall blurring effect can be expressed as a special form of a convolution operation of the 3D density with a kernel defined on $SE(3)$, the Lie group of rigid body motions in 3D. We call this form of convolution mixed spatial-motional convolution. We discuss the ill-conditioned nature of the deconvolution needed to deblur the reconstructed 3D density in terms of parameters associated with the unknown probability in $SE(3)$. We provide an algorithm for recovering the conformational information of large multi-unit biomolecular complexes (essentially deblurring) under certain biologically plausible prior structural knowledge about the subunits of the complex in the case the blurring kernel has a special form.

1 Introduction

Reconstructing three dimensional densities associated with large biomolecular complexes using single particle 3D Electron Microscopy (EM) has proved very promising in structural biology and other biological applications. The reader is referred to [4] for general introduction and extensive references.

At the core of single particle reconstruction lies the problem of reconstruction of a 3D volume from thousands of very noisy 2D projections of the volume formed along *random* (*unknown*) projection directions relative to the body-fixed frame of the biomolecular complex. What makes this problem different from standard tomography is exactly the fact that the projection directions are unknown and need to be determined before one can apply a standard 3D reconstruction such as weighted back-projection. In addition, due to certain biological restrictions the signal to noise ratio in a single projection image is extremely low (e.g., typically

F. Nielsen and F. Barbaresco (Eds.): GSI 2015, LNCS 9389, pp. 643–653, 2015.
DOI: 10.1007/978-3-319-25040-3_69

at the order of 1/100). The reason one has to deal with such random projections is that in single particle EM imaging (specifically cryo-EM) one essentially takes a 2D image of a layer of a frozen sample containing a large number of copies or instances of a biomolecular complex lying at random positions and orientations within the sample. The output of a reconstruction algorithm is a *blurred* 3D (so-called) *density* map representing the Coulomb potentials of the atoms of the biomolecular complex under experiment improve our algorithm [4].

In this paper (in Sect. 2) we study two sources of blurring: the first one is due to variations in the structure or conformational states of the biomolecular complex in the sample (i.e., not all instances of the biomolecular complex are exactly the same). The second source of blurring is due to errors introduced in the process of reconstructing the 3D density from the collected images. We first show that each of these blurring effects can be modeled as a specific form of averaging or convolution of the ground truth 3D volume with probability density (kernel) defined on $SE(3)$, the group of rigid body motions. The associated *blind deblurring* or *deconvolution* is severely ill-posed and requires prior information or information (fusion) from other imaging modalities to yield a well-posed problem. In certain cases of dealing with large multi-unit complexes, however, one may have information about the shape of the subunits and the problem recovering the shape of the complex basically boils down to recovering the relative positions of the subunits. In Sect. 3 we derive a set of equations describing blurring of a rigid body model under a $SE(3)$ kernel in terms of the body parameters and the parameters of the kernel (in particular its Lie-algebraic $SE(3)$ *mean* and *covariance*). We also derive a simple algorithm for recovering conformational information under the assumption of *isotropic* blurring and we show the application of this algorithm to simulated data; and we conclude the paper in Sect. 4. We mention that closely related works include [6] and [7], where, respectively, Eculidean convolution and spherical convolution have been employed to model the blurring effects.

2 Blurring as Mixed Spatial-Motional Convolution

In this section we study two sources of blurring effects in 3D single particle EM, both of which can be modeled using probability densities on $SE(3)$. The first effect is conformational blurring within a biomolecular complex due to internal motions. The second is blurring during the process of reconstructing 3D densities from an ensemble of noisy 2D projections. As an idealization, we assume that these effects can be treated independently.

The preparation of the sample for single particle EM usually starts with a solution containing the designated biomolecular complex, each consisting of multiple macromolecules, and freezing the solution in the form of a very thin layer. For various reasons the instances of the biomolecular complex in the sample may not have exactly the same shape. For example, they may be at different conformational states (e.g., open or close) or their subunits might have been

displaced in the freezing process. Let us consider a biomolecular complex with 3D density ρ consisting of N macromolecular subunits

$$\rho(\mathbf{r}) = \sum_{i=1}^{N} \rho_i(\mathbf{r}), \tag{1}$$

where $\rho_i : \mathbb{R}^3 \to \mathbb{R}$ is the 3D density of subunit i. Often in large biomolecular complexes we may model ρ_i as a rigid body. In this case, we model the effect of conformational states or motions as the ensemble or average of the *action* of $SE(3)$ on the rigid bodies. Specifically, let $\cdot$ denote the standard $SE(3)$ action in $\mathbb{R}^3$

$$r \mapsto g \cdot \mathbf{r} = R\,\mathbf{r} + t, \tag{2}$$

where each $g \in SE(3)$ is represented with the rotation-translation pair $(R, t) \in SO(3) \times \mathbb{R}^3$, and the group operation for $SE(3)$ is $g_1 \circ g_2 = (R_1 R_2, g_1 \cdot t_2)$. Then a copy (or instance) of subunit $i \geq 2$ with density ρ_i might be under transformation g relative to the subunit $i = 1$, which can be described in the global (lab) coordinates as $\rho_i(g^{-1} \cdot \mathbf{r})$. Throughout the sample the copies might go through different transformations which we model by a $SE(3)$ probability density $f_i : SE(3) \to \mathbb{R}$ and the ensemble average of such motional or conformational variations can be modeled as

$$\tilde{\rho}_i(\mathbf{r}) = (f_i \star \rho_i)(\mathbf{r}) := \int_{SE(3)} f_i(g)\rho_i(g^{-1} \cdot \mathbf{r})dg \tag{3}$$

where dg is the Haar measure for $SE(3)$. The above operation may be called *mixed spatial-motional* convolution. The operation resembles convolution on $SE(3)$,

$$(k * f_i)(g) := \int_{SE(3)} k(h) f_i(h^{-1} \circ g)dh,$$

which we denote with an asterisk $*$ rather than a $\star$, but $f_i \star \rho_i$ is not a convolution since the functions under operation have different domains.

The total conformationally blurred 3D density with body 1 fixed can then can be expressed as

$$\tilde{\rho}(\mathbf{r}) = \sum_{i=1}^{N} \tilde{\rho}_i(\mathbf{r}) = \sum_{i=1}^{N} (f_i \star \rho_i)(\mathbf{r}). \tag{4}$$

In the above f_1 is assumed to be the Dirac delta function at the identity of $SE(3)$, denoted by $\delta(g)$. As far as cryo-EM imaging is concerned, (3) and hence (4) show non-physical ensemble averages, since they are not directly measured. This is in contrast to Small-Angle-X-ray-Scattering (SAXS) measurements in which the ensemble average is measured directly [3]. Here, the actual averaging or superposition of the different (continuum of) conformational states is to happen in the reconstruction process (algorithm). Specifically, in the imaging step, many copies of the biomolecular complex in each conformational state, positioned and oriented randomly throughout the sample, are imaged *separately*.

Then, these 2D images are fed to a 3D reconstruction algorithm to reconstruct a 3D density. Therefore, one expects that the ensemble averaging should happen in the reconstruction process. However, this also means that what a specific algorithm does may matter. We first consider an idealized algorithm (meaning that the algorithm introduces no errors). We also assume that we have an algorithm designed to deal with homogeneous samples. Most commonly used algorithms are such and they assume a single conformational state of the biomolecular complex in the sample. To be compatible with this assumption we also assume that the probability densities associated with conformational state variation (f_i's) are unimodal and concentrated enough (i.e., small conformational variations within the sample). Before proceeding further, we mention that the problem of heterogeneity of data is a challenging problem in single particle reconstruction, which in reality limits the accuracy of these methods [4, p. 266], [5]. Source of heterogeneity could range from impurity in the sample to presence of ligands and different conformational states. The latter is our main focus here. Here, we have distinguished between large and small variation in conformational states. The presence of large deviations in conformational states essentially is equivalent to a multi-modal or non-concentrated distribution f_i. The existence of such modes or classes makes the 3D reconstruction problem much more difficult. Specifically, the step of classification of the images will be very hard for heterogeneous data due to the intermingling between variation in pose and conformational state as portrayed on the 2D projections ([5], and see below). Nevertheless, specific algorithms for heterogeneous data have been developed (see e.g., [11]), but the subject is still in its fancy [5].

In the rest of discussion for convenience we consider a biomolecular complex comprised of only two subunits $\rho(\mathbf{r}) = \rho_1(\mathbf{r}) + \rho_2(\mathbf{r})$, and we assume that its conformational states are determined only by a single copy of $SE(3)$, i.e., the total density under a conformational state change $g \in SE(3)$ is $\rho_g(\mathbf{r}) = \rho_1(\mathbf{r}) + \rho_2(g^{-1} \cdot \mathbf{r})$. We assume that g has the $SE(3)$ probability density f. A typical biomolecular complex in the frozen sample will be $\rho_g(h^{-1} \cdot \mathbf{r})$, where $h = (R_h, t_h) \in SE(3)$ denotes a random orientation (pose) and position of the biomolecular complex in the sample. Henceforth we use the following notation:

$$\rho_g^h(\mathbf{r}) := \rho_g(h^{-1} \cdot \mathbf{r}) = \rho(g^{-1} \cdot (h^{-1} \cdot \mathbf{r})) = \rho((h \circ g)^{-1} \cdot \mathbf{r}).$$

In the imaging process an image from each copy of $\rho_g^h(\mathbf{r})$ is formed by the projection operation (along the z axis)

$$p_g^h(x, y) = \int \rho_g^h(\mathbf{r}) dz \tag{5}$$

where $\mathbf{r} = [x, y, z]^\top$. A typical (homogeneous) 3D reconstruction algorithm first brings all the 2D images to a common origin, which we assume is the origin of the lab frame. Due to the large amount of noise in these images, they are class averaged. This process can be described as an in-plane $SE(2)$ blurring [8,9]. A class is meant to correspond to the biomolecular complex being imaged along similar directions (ideally exactly the same direction). This means that a class

roughly corresponds to images from the copies of the biomolecular complex in the sample that are at the same *orientation*, i.e., a full 3D rotation modulo an in-plane rotation in the $x - y$ plane.

The next step is finding the actual projection direction for each class relative to the body-fixed frame of the biomolecular complex. This is known as *angular reconstitution* (see [12,14] and references therein for related methods). Assuming the angles are found correctly, the actual 3D reconstruction is the standard tomographic reconstruction. Often the *weighted backprojection* algorithm is used, which given enough number of sampled projection directions can reconstruct the 3D volume without any aliasing [4]. In our case this means that the ensemble average $\tilde{\rho}(\mathbf{r})$ is reconstructed. Hence, although, as mentioned before, $\tilde{\rho}(\mathbf{r})$ in (4) is a non-physical ensemble average, it can be realized in the 3D reconstruct due to the fact that the 2D images are averaged from many of copies of the biomolecular complex at different conformational states and also the fact that the steps involved in the reconstruction are linear operations. Notice, however, that this is under the assumption of the steps of centering the 2D projection, classification, and angular reconstitution are error free. In reality, all these steps are highly prone to error due to the extremely high level noise in the image formation process. Additionally, notice that a possible interplay between g and h can result in complications in the classification step. However, also note that whether such an interplay (and the ensued misclassification) necessarily results in reconstruction errors also depends on the structure of the complex (e.g., if certain symmetries exist then the misclassification won't be harmful).

We postulate that the output of the 3D reconstruction is a version of the conformationally blurred density $\tilde{\rho}$, where an additional $SE(3)$ blurring kernel includes both motional blurring due to class averaging and reconstruction errors. That is, the contribution to the blurred density of the biomolecular complex from the i^{th} macromolecular subunit will be of the form

$$\tilde{\tilde{\rho}}_i(\mathbf{r}) = (k \star \tilde{\rho}_i)(\mathbf{r}) = (k \star (f_i \star \rho_i))(\mathbf{r}) = ((k * f_i) \star \rho_i)(\mathbf{r}).$$

Here $k : SE(3) \to \mathbb{R}$ is the reconstruction blurring kernel that contains contributions from both class averaging effects and 3D reconstruction.

Of course, we state this under certain assumptions most notably that conformational states and projections orientations do not interplay and that error kernels are independent of the poses. Both assumptions are plausible under small conformational variation and if many different poses are available. We also add that in many image processing applications modeling blurring using a convolution is a viable and common approach (independent of the source and mechanism of the blurring which could be highly nonlinear). However, the more challenging part is the fact that the kernel is unknown and hence one has to resort to blind de-convolution methods.

3 Recovering Conformational Information Based on Moment Matching

Blind deconvolution or deblurring, in general, without prior information is ill-posed and difficult. In certain biological applications the goal is to understand the conformational state of a large biomolecular complex comprised of subunits, while the structure of each of subunit is a-priori *known*, and the goal is to find the relative position (pose) of the subunits with respect to each other. For example, given a complex comprised of two subunits the goal might be to decide whether it is in close or open configuration or to find the relative position of the two subunits. We assume that each subunit can be modeled by a rigid body, in particular, an ellipsoid itself modeled by a Gaussian in $\mathbb{R}^3$. This, in particular, means that in (1) ρ_i's are assumed to be known up to a rotation and translation. Furthermore, we assume that upon reconstruction we can separate the reconstructed subunits $\tilde{\rho}_i$ from each other. This may be done through a 3D segmentation algorithm, manually, or using a clustering algorithm such k-means. The extent to which this assumption is practical or valid depends on the problem and needs further verification. Assuming these simplifications, in the following we will consider blurring a 3D Gaussian distribution with an $SE(3)$ kernel and find the mean and covariance of the blurred density in terms of the parameters (mean and covariance) of the kernel and the density.

Parameterization of $SE(3)$ Kernel. Let $\mathfrak{se}(3)$ denote the Lie algebra of $SE(3)$. Also let $\exp : \mathfrak{se}(3) \to SE(3)$ denote the matrix exponential and $\log : SE(3) \to \mathfrak{se}(3)$ its inverse. Recall that an element $\Omega \in \mathfrak{se}(3)$ can be represented as $\Omega = \left[\begin{array}{c|c} \Omega_R & \omega_t \\ \hline 0 & 0 \end{array}\right]$, where Ω_R is a 3×3 skew-symemtri matrix and $\omega_t \in \mathbb{R}^3$. We will need the following well-known fact which gives a closed form expression for the logarithm map (see e.g., [10] for a proof):

Proposition 1. *Let* $\Omega = \left[\begin{array}{c|c} \Omega_R & \omega_t \\ \hline 0 & 0 \end{array}\right] \in \mathfrak{se}(3)$. *Then* $e^{\Omega} = \left[\begin{array}{c|c} e^{\Omega_R} & \frac{e^u-1}{u}\big|_{u=\Omega_R}\ \omega_t \\ \hline 0 & 1 \end{array}\right]$. *Conversely if* $g = \left[\begin{array}{c|c} R & t \\ \hline 0 & 1 \end{array}\right] \in SE(3)$, *then* $\log(g) = \left[\begin{array}{c|c} \log(R) & \frac{u}{e^u-1}\big|_{u=\log(R)}\ t \\ \hline 0 & 0 \end{array}\right] \in \mathfrak{se}(3)$. *This result holds if all the eigenvalues of* Ω *are less than* π *in absolute value or equivalently* g *has no eigenvalue of* -1.

We now define the notion of Lie-algebraic mean [13] (also known as bi-invariant mean [1,10]) and covariance [2] for $SE(3)$-valued random variables:

Definition 1. *Let* $\mathbf{g}$ *be an* $SE(3)$*-valued random variable with probability density* $f : SE(3) \to \mathbb{R}$. *Then we define a mean* $\mu_{\mathbf{g}}$ *of* $\mathbf{g}$ *as a solution to*[1]

$$\mathbb{E}\{\log(\mu_{\mathbf{g}}^{-1} g)\} = \int_{SE(3)} \log(\mu_{\mathbf{g}}^{-1} g) f(g) dg = 0 \tag{6}$$

[1] Here $\mu_{\mathbf{g}}$ and $\Sigma_{\mathbf{g}}$ are not functions of g, but are properties of the random variable $\mathbf{g}$ that has distribution $f(g)$.

and the associated covariance $\Sigma_{\mathbf{g}}$

$$\Sigma_{\mathbf{g}} := \mathbb{E}\{\text{vec}(\Omega_g)\text{vec}(\Omega_g)^\top\} = \int_{SE(3)} \text{vec}(\Omega_g)\text{vec}(\Omega_g)^\top f(g)dg \tag{7}$$

where vec : $\mathfrak{se}(n) \to \mathbb{R}^6$ *is an isomorphism between* $\mathfrak{se}(3)$ *and* $\mathbb{R}^6$ *and* $\Omega_g = \log(g\mu_{\mathbf{g}}^{-1})$.

Due to topological constraints the Eq. (6) for mean has always at least two solutions on $SE(3)$. However, it can be shown that if f is concentrated in a small enough region, then there exists a unique mean in that region [10]. To our knowledge stronger results are not known. The covariance $\Sigma_{\mathbf{g}}$ depends on the isomorphism used. We use the standard isomorphism induced by the basis

$$E_1 = \begin{bmatrix} 0&0&0&0\\ 0&0&-1&0\\ 0&1&0&0\\ 0&0&0&0 \end{bmatrix}, E_2 = \begin{bmatrix} 0&0&1&0\\ 0&0&0&0\\ -1&0&0&0\\ 0&0&0&0 \end{bmatrix}, E_3 = \begin{bmatrix} 0&-1&0&0\\ 1&0&0&0\\ 0&0&0&0\\ 0&0&0&0 \end{bmatrix}, \tag{8a}$$

$$E_4 = \begin{bmatrix} 0&0&0&1\\ 0&0&0&0\\ 0&0&0&0\\ 0&0&0&0 \end{bmatrix}, E_5 = \begin{bmatrix} 0&0&0&0\\ 0&0&0&1\\ 0&0&0&0\\ 0&0&0&0 \end{bmatrix}, E_6 = \begin{bmatrix} 0&0&0&0\\ 0&0&0&0\\ 0&0&0&1\\ 0&0&0&0 \end{bmatrix}. \tag{8b}$$

Thus, if $\Omega = \sum_{i=1}^{N} \omega_i E_i$, then we have $\text{vec}(\Omega) = (\omega_1, \cdots, \omega_6)^\top \in \mathbb{R}^6$.

Mean and Covariance of the Blurred 3D Density. Consider the model:

$$\mathbf{y} = \mathbf{R}\mathbf{r} + \mathbf{t},\ \mathbf{r} \in \mathbb{R}^3,\ \mathbb{E}\{\mathbf{r}\} = 0, \mathbb{E}\{\mathbf{r}\mathbf{r}^\top\} = C_{\mathbf{r}}, g = \left[\begin{array}{c|c} \mathbf{R} & \mathbf{t} \\ \hline 0 & 1 \end{array}\right] \in SE(3), \tag{9}$$

with $\mathbf{g}$ and $\mathbf{r}$ being statistically independent. This model corresponds to the mixed spatial-motional convolution (3). The goal is to express the Euclidean mean and covariance matrix of $\mathbf{y}$ (which we assumed can be estimated from blurry 3D reconstruction) in terms of covariance $C_{\mathbf{r}}$ (which we assumed is given) and $SE(3)$ mean and covariance of $\mathbf{g}$ which are to be estimated. Denote the $SE(3)$-mean of $\mathbf{g}$ by $\mu_{\mathbf{g}}$, where $\mu_{\mathbf{g}} = \left[\begin{array}{c|c} \mu_{\mathbf{R}} & \mu_{\mathbf{t}} \\ \hline 0 & 1 \end{array}\right]$. Note that $\int \log(\mu_{\mathbf{g}}^{-1} g) f(g)dg = 0$ implies that $\int \mu_{\mathbf{g}}^{-1} \log(g\mu_{\mathbf{g}}^{-1})\mu_{\mathbf{g}} f(g)dg = 0$ and $\int \log(g\mu_{\mathbf{g}}^{-1}) f(g)dg = 0$, hence

$$g = e^{\log(g\mu_{\mathbf{g}}^{-1})}\mu_{\mathbf{g}} = e^{\Omega_g}\mu_{\mathbf{g}},\ \mathbb{E}\{\Omega_g\} = 0,\ \text{where } \Omega_g = \log(g\mu_{\mathbf{g}}^{-1}) = \left[\begin{array}{c|c} \Omega_R & \omega_t \\ \hline 0 & 0 \end{array}\right] \in \mathfrak{se}(3). \tag{10}$$

The following proposition gives the first two moments of $\mathbf{y}$ up to 2^{nd} order terms in terms of those of $\mathbf{r}$ and $\mathbf{g}$. The proof is straightforward using Proposition 1 and some algebraic manipulation.

Proposition 2. *Under statistical independence of rotation and translation at the Lie algebra (i.e., independence of* $\mathbf{\Omega}_R$ *and* ω_t *in* (10)*) and statistical independence of* g *and* $\mathbf{r}$ *the forward equations for the mean and covariance of* $\mathbf{y}$ *in* (9) *up to second order are:*

$$\mathbb{E}\{\mathbf{y}\} = \mathbb{E}\{\mathbf{t}\} \overset{2nd}{=} (I + \frac{1}{2}\mathbb{E}\{\Omega_R^2\})\mu_{\mathbf{t}} \tag{11a}$$

$$C_{\mathbf{y}} = \mathbb{E}\{RC_{\mathbf{r}}R^\top\} + C_{\mathbf{t}} \overset{2nd}{=} \tilde{C}_{\mathbf{r}} + \mathbb{E}\{\Omega_R\tilde{C}_{\mathbf{r}}\Omega_R^\top\} + \frac{1}{2}\mathbb{E}\{\Omega_R^2\}\tilde{C}_{\mathbf{r}} + \frac{1}{2}\tilde{C}_{\mathbf{r}}\mathbb{E}\{\Omega_R^2\} + \mathbb{E}\{\Omega_R\mu_t\mu_t^\top\Omega_R^\top\} + \mathbb{E}\{\omega_t\omega_t^\top\} \tag{11b}$$

where $\tilde{C}_{\mathbf{r}} = \mu_R C_{\mathbf{r}}\mu_R^\top$ *and the expectations of quantities quadratic in* Ω_R *and* ω_t *can be expressed in terms of the* $SE(3)$ *covariance of* g*, i.e.,* $\Sigma_{\mathbf{g}}$ *in* (7)*.*

Simplified Equations Under Isotropic Blurring. The unknowns in (11) are the 6×6 covariance matrix $\Sigma_{\mathbf{g}}$ and the 6×1 vector $\mu_{\mathbf{g}}$, which in general amounts to 27 unknowns, whereas the number of independent equations is 9. However, if we assume that blurring is isotropic in translational and rotational directions, i.e., $\Sigma_{\mathbf{g}}$ is diagonal and variances along E_1, E_2 and E_3 are equal to σ_R^2 and along E_4, E_5 and E_6 are σ_t^2, then the number of unknowns will be 8. Thus, we have

$$\mathbb{E}\{\mathbf{y}\} = \mathbb{E}\{\mathbf{t}\} \overset{2nd}{=} (1 - \sigma_R^2)\mu_{\mathbf{t}} \tag{12a}$$

$$C_{\mathbf{y}} \overset{2nd}{=} \mu_{\mathbf{R}}C_{\mathbf{r}}\mu_{\mathbf{R}}^\top + \sigma_{\mathbf{R}}^2\big(\mathrm{tr}(C_{\mathbf{r}})I_3 - 3\mu_{\mathbf{R}}C_{\mathbf{r}}\mu_{\mathbf{R}}^\top\big) + \sigma_{\mathbf{R}}^2\big(\|\mu_{\mathbf{t}}\|^2 I_3 - \mu_{\mathbf{t}}\mu_{\mathbf{t}}^\top\big) + \sigma_{\mathbf{t}}^2 I_3, \tag{12b}$$

where I_3 is the 3×3 identity matrix. The interesting point here is that if μ_t is large (even for small rotational noise σ_R^2) $C_{\mathbf{y}}$ can become large merely due to large translational mean. Considering our argument about blurring due to 3D reconstruction errors the assumption of isotropic blurring might not be justified, nevertheless, as a starting point to solve the inverse problem in Proposition 2 we choose this assumption. Figure 1a shows the blurring effect of an istropic $SE(3)$ kernel with mean $\mu_{\mathbf{g}} = I_4$, $\sigma_{\mathbf{R}} = \pi/10$ and $\sigma_{\mathbf{t}} = \frac{1}{10}$ applied to a unit vector along the z-direction in $\mathbb{R}^3$.

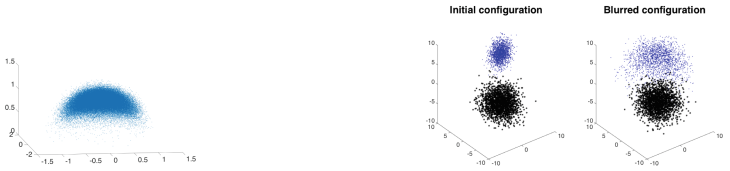

(a) Example of blurring by an isotropic $SE(3)$ kernel.

(b) The right panel shows the blurred version of right configuration in our numerical simulation.

Fig. 1. Examples of blurring under $SE(3)$ kernels.

Algorithm. The two equations in (12) are coupled and nonlinear in the unknowns; however, by fixing σ_R^2 in (12a) and μ_t in (12b) they decouple. Thus,

in the first step, we find μ_t from (12a) (fixing σ_R^2) and in the next step $\mu_R, \sigma_R^2, \sigma_t^2$ from (12b) using min-square fitting, and iterate these steps. Specifically, based on (12b) we consider the cost function

$$\begin{aligned} &F(\mu_R, \sigma_R^2, \sigma_t^2) \\ &= \|\mu_R C_{\mathbf{r}} \mu_R^\top + \sigma_R^2(\mathrm{tr}(C_{\mathbf{r}}) I_3 - 3\mu_R C_{\mathbf{r}} \mu_R^\top) + \sigma_R^2(\|\mu_t\|^2 I_3 - \mu_t \mu_t^\top) + \sigma_t^2 I_3 - C_{\mathbf{y}}\|_F^2, \end{aligned} \tag{13}$$

where $\|\cdot\|_F$ is the Frobenius norm. We solve the regularized minimization

$$\min_{\mu_R \in SO(3), \sigma_R^2, \sigma_t^2} F_r(\mu_R, \sigma_R^2, \sigma_t^2; \lambda_R, \lambda_t) \tag{14}$$

where $F_r(\mu_R, \sigma_R^2, \sigma_t^2; \lambda_R, \lambda_t) = F(\mu_R, \sigma_R^2, \sigma_t^2) + \lambda_R(\sigma_R^2)^2 + \lambda_t(\sigma_t^2)^2$ and $\lambda_R, \lambda_t > 0$ are small regularization weights. Our experiments show that although the number of unknowns is more than the number of equations in (12a) and (12b), still sensitivity can be high; thus we add the regularization terms in this minimization. Solving (14) in an *alternative* minimization fashion results in simple (closed-form) eigendecomposition-based solution for μ_R and scalar min-square solution with thresholding to enforce $\sigma_R^2, \sigma_t^2 \geq 0$.

Numerical Simulations. We simulate a complex with two subunits ρ_1 and ρ_2 modeled with two Gaussians $\mathbf{r}_1$ and $\mathbf{r}_2$ with covariances $C_{\mathbf{r}_1} = \mathrm{diag}(3, 2, 1)$ and $C_{\mathbf{r}_2} = \mathrm{diag}(4, 3, 5)$, respectively. We consider two $SE(3)$ blurring kernels with

$$\mu_{\mathbf{g}_1} = \begin{bmatrix} 0.6063 & 0.3861 & -0.6952 & 5.0000 \\ -0.7453 & -0.5807 & 0.3275 & 5.0000 \\ -0.2773 & 0.7167 & 0.6399 & 5.0000 \\ 0 & 0 & 0 & 1.0000 \end{bmatrix}, \mu_{\mathbf{g}_2} = \begin{bmatrix} -0.6196 & -0.3585 & -0.6983 & -1.0000 \\ -0.3601 & -0.6607 & 0.6587 & -3.0000 \\ -0.6975 & 0.6595 & 0.2802 & -2.0000 \\ 0 & 0 & 0 & 1.0000 \end{bmatrix} \tag{15}$$

and with variances $(\sigma_{R_1}^2, \sigma_{t_1}^2) = (0.2, .02)$ and $(\sigma_{R_2}^2, \sigma_{t_2}^2) = (.1, .01)$. We generate $T = 2000$ i.i.d. samples of $\mathbf{r}_i, \mathbf{g}_i$ $(i = 1, 2)$ and then $\mathbf{y}_i$ according to (9). The left panel in Fig. 1b shows the original configuartion and the right panel shows the blurred configuration, in which the subunits appear bloated (blue (or $\cdot$) and black (or *) correpond to $\mathbf{r}_1$ and $\mathbf{r}_2$, respectively). We run a k-means algorithm to separate the two clouds (subunits). Using the above algorithm with $\lambda_R = \lambda_t = 1$ to get the estimates:

$$\hat{\mu}_{\mathbf{g}_1} = \begin{bmatrix} -0.7361 & 0.4145 & -0.5351 & 4.7676 \\ -0.3606 & -0.9092 & -0.2082 & 4.8539 \\ -0.5728 & 0.0397 & 0.8187 & 4.7737 \\ 0 & 0 & 0 & 1.0000 \end{bmatrix}, \hat{\mu}_{\mathbf{g}_2} = \begin{bmatrix} -0.6596 & -0.5253 & -0.5375 & -0.9976 \\ -0.2048 & -0.5625 & 0.8010 & -3.0366 \\ -0.7232 & 0.6384 & 0.2635 & -2.0821 \\ 0 & 0 & 0 & 1.0000 \end{bmatrix} \tag{16}$$

and $\hat{\sigma}_{R_1}^2 = 0.15$, $\hat{\sigma}_{t_1}^2 = 0.89$, $\hat{\sigma}_{R_2}^2 = 0.11$, and $\hat{\sigma}_{t_2}^2 = 0.09$. There is an indeterminacy in estimating $\mu_{\mathbf{g}}$ in the form of a rotation by π, i.e., a factor of the form $\Pi = \left[\begin{smallmatrix} -1 & 0 & 0 \\ 0 & -1 & 0 \\ 0 & 0 & 1 \end{smallmatrix}\right]$ and its permutations. After fixing the indeterminacy, we get $d(\mu_{R_1}, \hat{\mu}_{R_1}) = 0.2491\pi$ and $d(\mu_{R_2}, \hat{\mu}_{R_2}) = 0.0751\pi$, where $d(\cdot, \cdot)$ is the standard Riemannian distance on $SO(3)$. Thus, the error in estimating $\mu_{\mathbf{g}}$ is low; however, estimating σ_R^2 and σ_t^2 is more difficult. Nevertheless, note that $\mu_{\mathbf{g}}$ is the more important or informative variable in determining relative configurations.

4 Conclusions

In this paper we reproted preliminary studies for the modeling of blurring effects in 3D reconstruction of densities in single particle EM using $SE(3)$ blurring kernels. We derived a set of blurring equations relating the parameters of the original 3D density and the blurring kernel to quantities which can be calculated from the reconstructed density. The equations are highly ill-posed to invert. However, in the case of a multi-unit complex one might have prior knowledge about the shape of the subunits. We examined this in the case of isotropic blurring and derived a simple regularized minimization algorithm to find conformational information of the complex (i.e., the relative positions of subunits). We plan to improve our algorithm e.g., by using more prior information and better regularizations.

Acknowledgements. Research reported in this publication was supported by the National Institute of General Medical Sciences of the National Institutes of Health under award number R01GM113240.

References

1. Arsigny, V., Pennec, X., Ayache, N.: Bi-invariant means in Lie groups. application to left-invariant polyaffine transformations (2006)
2. Chirikjian, G.S.: Stochastic Models, Information Theory, and Lie Groups. Springer, Boston (2012)
3. Feigin, L., Svergun, D.I., Taylor, G.W.: Structure Analysis by Small-angle X-ray and Neutron Scattering. Springer, Berlin (1987)
4. Frank, J.: Three-dimensional electron microscopy of macromolecular assemblies: Visualization of biological molecules in their native (2006)
5. Frank, J.: Story in a sample-the potential (and limitations) of cryo-electron microscopy applied to molecular machines. Biopolymers **99**(11), 832–836 (2013)
6. Hirsch, M., Schölkopf, B., Habeck, M.: A blind deconvolution approach for improving the resolution of cryo-EM density maps. J. Comput. Biol. **18**(3), 335–346 (2011)
7. Kishchenko, G.P., Leith, A.: Spherical deconvolution improves quality of single particle reconstruction. J. Struct. Biol. **187**(1), 84–92 (2014)
8. Park, W., Chirikjian, G.S.: An assembly automation approach to alignment of noncircular projections in electron microscopy. IEEE Trans. Autom. Sci. Eng. **11**(3), 668–679 (2014)
9. Park, W., Midgett, C.R., Madden, D.R., Chirikjian, G.S.: A stochastic kinematic model of class averaging in single-particle electron microscopy. Int. J. Rob. Res. **30**(6), 730–754 (2011)
10. Pennec, X., Arsigny, V.: Exponential barycenters of the canonical cartan connection and invariant means on Lie groups. In: Nielsen, F., Bhatia, R. (eds.) Matrix Information Geometry, pp. 123–166. Springer, Heidelberg (2013)
11. Scheres, S.H., Gao, H., Valle, M., Herman, G.T., Eggermont, P.P., Frank, J., Carazo, J.-M.: Disentangling conformational states of macromolecules in 3D-EM through likelihood optimization. Nature Methods **4**(1), 27–29 (2007)
12. van Heel, M., Gowen, B., Matadeen, R., Orlova, E.V., Finn, R., Pape, T., Cohen, D., Stark, H., Schmidt, R., Schatz, M., et al.: Single-particle electron cryo-microscopy: towards atomic resolution. Q. Rev. Biophys. **33**(04), 307–369 (2000)

13. Wang, Y., Chirikjian, G.S.: Error propagation on the Euclidean group with applications to manipulator kinematics. IEEE Trans. Robot. **22**(4), 591–602 (2006)
14. Zhao, Z., Singer, A.: Rotationally invariant image representation for viewing direction classification in cryo-EM. Journal of structural biology **186**(1), 153–166 (2014)